Cordycepin Improved Neuronal Synaptic Plasticity Through CREB-Induced NGF Up-Regulation Driven By Microglial M2 Polarization: A Symphony Communication Between Microglia and Neurons in AD

Linchi Jiao
China Medical University https://orcid.org/0000-0003-2205-2808
Mingyan Liu
China Medical University
Xin Zhong
China Medical University
Weifan Yao
China Medical University
Guowei Ma
China Medical University
Jiajia Shen
China Medical University
Yuqiang Wu
China Medical University
Ke Du
China Medical University
Junxiu Liu
China Medical University
Junhui Tong
China Medical University
Chao Liu
Liaoning Medical Diagnosis and Treatment Center
Jia Fu
Liaoning Medical Diagnosis and Treatment Center
Zhihua Yu
China Medical University
Minjie Wei (minjie_wei@163.com)
China Medical University https://orcid.org/0000-0001-5548-7280

Research article

Keywords: Cordycepin, microglial M2 polarization, CREB, NGF, Alzheimer's disease

Posted Date: February 12th, 2021

DOI: https://doi.org/10.21203/rs.3.rs-184003/v1

Abstract

Background: The purpose of this study was to explore the molecular mechanism of the neuroprotective effect of Cordycepin (CCS) on improving the neuro-immune microenvironment of AD neurons by mediating microglial M2 polarization.

Methods: We investigated microglial M2 polarization from M1, neuronal senescence, and synaptic plasticity by biological techniques such as animal behavior, cell biology, morphology, and bioinformatics.

Results: CCS improved learning and memory impairment in 9-month-old APP/PS1 mice. CCS induced the microglial M2 polarization, up-regulated the expression and secretion level of NGF, and inhibited neuronal apoptosis, senescence, and synaptic damage caused by abnormal microglial activation in vivo and in vitro. CREB was activated by the M2 polarization and mediated the NGF expression and secretion after CCS treatment. CREB bound with the *Sg3* promoter region of NGF (-1018~-1011), which increased NGF expression and secretion. CREB-induced NGF upregulation driven by microglial M2 polarization to improve the neuronal synaptic plasticity inhibits neuronal apoptosis and senescence. As a novel participant in the intercellular communication between MG and neurons, NGF contributed to the neuroprotective efficacy of CCS treatment.

Conclusions: CCS improved the neuronal synaptic plasticity and senescence by promoting microglial M2 activation driven by CERB-induced NGF upregulation and conducted the symphony communication of MG-Neuron in AD.

Background

Alzheimer's disease (AD) is one of the most common age-related neurodegenerative diseases(1, 2). The main clinical symptoms of AD are progressive cognitive impairment and decreased ability of learning and memory(3). For a long time, the relevant studies have mainly focused on the neuronal damage and degenerative changes caused by the deposition of Amyloid-β (Aβ) peptide as senile plaques and the abnormal accumulation of protein tau as neurofibrillary tangles(2, 4). However, recent studies have found that the neuroimmune microenvironment is of great significance for neuron fate. Microglia (MG), as the only immune cells in the central nervous system, can be caused by MG phenotypic transformation after activation. Subsequently, various effectors secreted by the activated microglia of different phenotypes are induced, neuroinflammatory response and the functional remodeling will elicit(5, 6). It also contributes to the regulation of the neuroimmune microenvironment and cell-to-cell communication between MG and neurons. It then plays an essential role in the morphology, function, and plasticity of neurons. Therefore, it is of great significance to identify the key effectors releasing from MG and modulating the crosstalk between MG and neurons to explore the MG-mediated neuroimmune microenvironment's main regulatory mechanisms for the discovery of new therapeutic targets for AD and new potential compounds against AD.

Nerve growth factor (NGF), as a neurotrophic factor, produces neuroprotective effects on the differentiation, growth, nutrition, and support of neurons(7). Some studies have validated that the lack of NGF in the brain induced neuronal aging, dysfunction, and apoptosis(8). Our previous studies showed that there was NGF deficiency leading to neuronal apoptosis in the brains of APP/PS1 mice(9). Pharmacological intervention, such as EGCG treatment, increased NGF levels, decreased the deposition of Aβ, and improved learning and memory impairment(9, 10). It indicated that NGF might be the critical modulator orchestrating the symphony between MG and neurons in the occurrence and progression of AD. However, there is no literature on whether the secretion of NGF is related to different microglial phenotypes and what its mechanism is. Therefore, it is essential to find new drugs to increase the expression of NGF to protect neurons and improve learning and memory impairment.

Cordycepin (CCS) is the first nucleoside antibiotic isolated from *Cordyceps militaris*, extracted from the fruiting body of artificially cultivated *Cordyceps militaris*(11). CCS has been proved to have various biological functions, including antioxidant, antibacterial and anti-inflammatory, anti-tumor, immunomodulatory, hypoglycemic and lipid-lowering, and anti-aging(12-15). It had been reported that CCS inhibited neuronal apoptosis and reduced the ischemic area in the brain of mice under hypoxia and hypoglycemia(16). CCS could also reduce excitatory toxicity produced by excitatory amino acids, block free radicals, and improve the cerebral injury of ischemia/reperfusion(16, 17). Simultaneously, CCS treatment could also significantly prolong mice's survival time with cerebral ischemia and improve learning and cognitive impairment(18). However, it is not clear whether the protective effect produced by CCS treatment is related to the microenvironment changes of neurons regulated by microglial activation and whether NGF plays a pivotal role in the MG-Neuron communication after CCS treatment. Therefore, this study investigated the anti-AD effect of CCS both in LPS+IFNγ induced microglia in vitro and APP/PS1 mice in vivo and deeply detected the neuroprotective effect of CCS and its related mechanism on neuroimmune microenvironment regulated by NGF induced by the microglial phenotypic transformation. It provides a new idea for the further study of MG-mediated neuroimmune microenvironment, builds a new basis of theoretical and experimental for discovering new anti-AD drugs, and finds some new targets for AD therapy.

Methods

Materials

All the cell culture reagents were purchased from Gibco (USA). CCS, LPS, Aβ1-42 were purchased from Sigma-Aldrich (USA). The IFNγ was purchased from Novus Biologicals (USA). The β-NGF recombinant protein was purchased from DAKEWE (China). The KG501, as a CREB inhibitor, was purchased from MedChemExpress (USA). The anti-IL-1β, TNF-α, iNOS, IL-10, TGF-β, Arg1, CREB, pCREB, NGF, β-Gal, GAP43, Syn, MAP2, NeuN, β-actin, β-tubulin, and GAPDH antibodies were obtained from Cell Signaling Technology (USA). The anti-Iba-1, NGF antibodies, and anti-NGF neutralizing antibodies were obtained from Abcam (USA). The anti-CD86 and CD206 antibodies were obtained from BD (USA). The HRP conjugated Rabbit anti-Goat IgG, Goat anti-Rabbit IgG, Goat anti-Mouse IgG, the FITC conjugated Donkey

anti-Rabbit IgG, and the TRITC conjugated Donkey anti-Goat IgG secondary antibodies were purchased from EarthOx Life Science (USA). The plasmids of CREBcDNA, NGF wild type, and NGF mutated type were obtained from Genewiz (China). The primer of IL-1β, TNF-α, iNOS, IL-10, TGF-β, Arg1, NGF, and SanPrep Column Plasmid DNA Extraction kit were obtained from Sangon Biotechnology (China). The Reverse Transcription Master Mix was purchased from TOYOBO (Japan). The TB Green Realtime PCR Master Mix was purchased from TaKaRa (Japan). The polyvinylidene difluoride membrane and enhanced chemiluminescent kit (ECL+) were purchased from Millipore (Germany). The Luciferase Report kit was obtained from Promega (USA). The RIPA buffer, DAPI, BCA, the Chromatin Immunoprecipitation, the Senescence-associated β- Galactosidase Staining, and the Annexin -FITC/Propidium Iodide (PI) Apoptosis kits were purchased from Beyotime Biotechnology (China). The CCK8 kit was purchased from Dojindo (Japan). The IL-1β, IL-10, and NGF activity assay kits were obtained from Nanjing Jiancheng Bioengineering Institute (China). All the other reagents were of analytical grade. All supplies are purchased from Jet (China).

Cell Line and Treatment

Mouse microglial cell line BV2 and rat pheochromocytoma cell line PC-12 was purchased from the Institute of Basic Medical Sciences of the Chinese Academy of Medical Sciences (China). BV2 cells were grown in Dulbecco's modified Eagle's media (DMEM), supplemented with 10% Fetal Bovine Serum (FBS) and 100 U mL^{-1} of penicillin-streptomycin in a 37°C, 5% CO_2 incubator. And PC-12 cells were grown in Dulbecco's modified Eagle's media (DMEM), supplemented with 5% Fetal Bovine Serum (FBS), 10% horse serum (HS), and 100 U mL^{-1} of penicillin-streptomycin in a 37°C, 5% CO_2 incubator. And 293T cells were grown in Dulbecco's modified Eagle's media (DMEM), supplemented with 10% Fetal Bovine Serum (FBS) and 100 U mL^{-1} of penicillin-streptomycin in a 37°C, 5% CO_2 incubator. Cells at passage 5–20 were used for the experiments. The Aβ1-42 peptide was used after 7 days of incubation at 37°C.

CCS stock solution was prepared in sterile double distilled water at a final concentration of 1 mg·mL-1, and then aseptically dispensed and immediately stored at -20 °C. 24 h after plating the BV2 cells, CCS stock solution was added to the media to a final concentration of 0.1 μg·mL^{-1}, 0.5 μg·mL^{-1}, 1 μg·mL^{-1} for 1 h in the CCS group. Then, the cells were treated with LPS (1 μg·mL^{-1}) for 1 h, and IFNγ (20 ng·mL^{-1}) for 6 h both in the LPS+IFNγ group and the CCS group, the cells in the control group were treated with cell culture media at the same volume.

BV2 cells were plated in 6-well plates for 24 h. And then, BV2 cells were treated with CCS (1 μg·mL^{-1}), LPS (1 μg·mL^{-1}), IFNγ (20 ng·mL^{-1}), rNGF (50 ng·mL^{-1}) or Neutralizing anti-NGF (0.05 μL·mL^{-1}) in different groups for 24 h. After treating BV2 cells for 24 h, cells were replaced with a complete medium for 24 h. The supernatant of the BV2 cells is used as a conditioned medium for PC-12 cells. Synchronously, PC-12 cells were treated with rNGF (50 ng·mL^{-1}) in 6-well plates for 48 h so that PC-12 cells would be induced into PC-12 neuronal cells. Next, PC-12 neuronal cells as neurons were treated with or without Aβ1-42 for

24 h. Finally, the supernatant of BV2 cells was cultured into PC-12 neuronal cells with or without Aβ1-42 as a conditioned medium and cultured for 24 h to detect.

Transfection

BV2 cells were plated in 6-well plates for 24 h. After 24 h, transient transfection of plasmids into BV2 cells was performed using Lipofectamine 3000 transfection reagent (Invitrogen by Thermo Fisher Sci.) according to the manufacturer's instructions. Next, the transfection medium was placed in the corresponding group for 24 h and then tested.

Animals and Treatments

The original APP/PS1 double-transgenic mice were obtained from the Jackson Laboratory [B6. Cg-Tg (APPswe, PSEN1dE9) 85Dbo/J]. The C57BL/6 mice were obtained from the Laboratory Animal Center of China Medical University. All animal care and experimental procedures were in line with the Laboratory Animal Ethical Standards of China Medical University and the Standard Medical Laboratory Animals' Care and Use Protocols.

9-month-old double-transgenic APP/PS1 mice were randomly assigned into two groups: APP/PS1 group (n=8) and CCS group (n=8). Age-matched C56BL/6 littermates were assigned as Wild Type (WT) group (n=8). And we must make sure that each group is half male. CCS (10 $mg \cdot kg^{-1} \cdot day^{-1}$) was intragastrically received in the CCS group; simultaneously, the same volume of distilled water was intragastrically administered in APP/PS1 group and WT group once daily for 4 weeks.

Behavioral Experiment

Morris Water Maze

Mice were given Morris water maze (MWM) for consecutive 6 days, including navigation tests and a probe trial test, as previously described with a few modifications. The Morris water maze is a stainless-steel circular water tank (120 cm diameter × 50 cm height) equipped with a platform (10 cm diameter) placed in the second quadrant and submerged 0.5 – 1 cm below the surface of the water. In brief, mice were allowed to swim freely for 1 min without the platform to adjust themselves to the baseline day's circumstances (day 0). From the 1st day to the 5th day, the platform was under the water in the tank for navigation tests, and each mouse was subjected to 4 trials per day at an inter-trial interval (ITI) of 1 min for spatial acquisition. Different start locations were used on each trial. If a mouse failed to find the platform within 1 min, it would be picked up and placed on the platform for 1 min. For each trial, the latency and the path length by which the mouse found the hidden platform was recorded. On the 6th day, a probe trial was performed to assess memory consolidation. In the trial, the platform was removed from the tank, and the mice were allowed to swim freely for 1 min to find the place of the original platform. Latency that each mouse spent in the quadrant and the frequency that each mouse crossed the center of

the quadrant (where the platform was previously located) were recorded. All the data were obtained by a video tracking system (Chengdu Taimeng Tech. Co. LTD, Chengdu, PR China).

Passive Avoidance test

Mice were subject to the passive avoidance test (PAT) using a PAT apparatus (BA-200, Chengdu Taimeng Tech. Co. LTD, Chengdu, PR China). In the training session, each mouse was put into the light compartment and allowed to explore for 3 min, at which point the guillotine door was raised to allow the mouse to enter the dark compartment. When the mouse entered the dark compartment, an electrical foot shock (voltage 36 V, 5 min) was delivered to make the mouse return to the light compartment. The training session was conducted before the test session. The test session was performed 24 h after the training session. In the test session, each mouse was placed in the light compartment and allowed to explore for 3 min, and then the guillotine door was raised. The latencies (s) and frequencies for mice to enter the dark compartment were recorded during the entire testing period (10 min). The latency of the mice that did not enter the dark compartment within 10 min was recorded as 600 s.

Step-down Avoidance test

The step-down avoidance test was employed to measure the retention of memory. A mouse was placed in a cylindrical insulation platform in a reaction box to adapt to the surrounding environment for 3 min. When the mouse stepped down from the platform, it would immediately receive an electric stimulation (voltage 30 V). In the 5 min training session, the mice would jump on the platform to prevent stimulation, and some mice might jump repeatedly. 24 h after training, the latency period (stepping down from the platform for the first time) and the number of errors (the frequency of jumping off the platform) were recorded.

Locomotivity test

The locomotivity test was conducted after other behavioral tests using a locomotivity testing paradigm (ZZ-6 system for mice, Chengdu Taimeng Tech. Co. LTD, Chengdu, PR, China). Briefly, mice were placed in the system, and the exploration was assessed for 5 min. Cages were routinely cleaned with ethanol following each session. The locomotivity and the frequency of stand-up for each mouse were recorded.

Transmission Electron Microscope (TEM)

After the animals' behavioral tests, the hippocampus tissues were separated immediately, and immersion fixation was completed at around 1 mm^3. Samples were rinsed in cold phosphate-buffered saline (PBS) and placed in 2.5% glutaraldehyde at 4 °C for 2 h. The tissues were rinsed in buffer and post-fixed with 1% osmium tetroxide for 2 h. The tissues were then rinsed with distilled water before undergoing a graded ethanol dehydration series and were infiltrated using a mixture of half acetone and half resin overnight at 4 °C. The tissues were embedded 24 h later in resin and cured fully, in turn, as follows: 37°C overnight, 45 °C for 12 h, and 60 °C for 24 h. After that, 70-nm sections were cut and stained with 3% uranyl acetate for

20 min and 0.5% lead citrate for 5 min. Ultrastructure changes of synapses in the hippocampus were observed under TEM (HITACHI H-7650).

Quantitative real-time PCR and RT-PCR

Total RNA from BV2 cells was extracted with TRIzon Reagent. RNA was reverse-transcribed to complementary DNA (cDNA) using the RT-PCR Quick Master Mix. And quantitative real-time PCR was performed according to the manufacturer's directions. After amplification, the PCR products were resolved by 2% agarose gel electrophoresis. For murine BV2 cells, primer sequences were listed as follows. The GAPDH gene was used as an internal control for IL-1β, TNF-α, iNOS, IL-10, TGF-β, Arg1, and NGF mRNA expressions analysis. And the results were analyzed using the $2^{-\Delta\Delta CT}$ method for quantification.

GAPDH, forward: 5'-AGCCTCGTCCCGTAGACAAAA-3',

reverse: 5'-TGGCAACAATCTCCACTTTGC-3';

IL-1β, forward: 5'-CCTGCAGCTGGAGAGTGTGGAT-3',

reverse: 5'-TGTGCTCTGCTTGTGAGGTGCT-3';

TNF-α, forward: 5'-AGCCCACGTCGTAGCAAACCAC-3',

reverse: 5'-AGGTACAACCCATCGGCTGGCA-3';

iNOS, forward: 5'-CCTTGGTGAAGGGACTGAGC-3',

reverse: 5'-CAACGTTCTCCGTTCTCTTGC-3';

IL-10, forward: 5'-GGTTGCCAAGCCTTATCGGAA-3',

reverse: 5'-TTCAGCTTCTCACCCAGGGA-3';

TGF-β, forward: 5'-GCAACAATTCCTGGCGTTACCTTG-3',

reverse: 5'-CAGCCACTGCCGTACAACTCC-3';

Arg1, forward: 5'-TGGGAATCTGCATGGGCAAC-3',

reverse: 5'-AGTGTTCCCCAGGGTCTACG-3';

NGF, forward: 5'-GCAGTGAGGTGCATAGCGTAA-3',

reverse: 5'-AGTGGGCTTCAGGGACAGAG-3'.

Western Blotting

BV2 cells, PC-12 cells, and the frozen hippocampus were homogenized, and the proteins were extracted and quantified with a BCA kit. For Western Blotting, the protein extracts of cells or tissues were separated on SDS-polyacrylamide gels and transferred to a polyvinylidene difluoride membrane. Next, the membrane was incubated with TBS containing 0.1% Tween-20 (TBST) with 5% bovine serum albumin for 1 h and then probed overnight at 4 °C with the following primary antibodies at the appropriate dilution: IL-1β, TNF-α, iNOS, IL-10, TGF-β, Arg1, NGF, pCREB, CREB, MAP2, NeuN, Syn, GAP43, β-Gal, β-tubulin, β-actin, GAPDH. After washing with TBST, the membranes were incubated with the corresponding secondary HRP-labeled antibody for 1 h at room temperature. After another TBST washing, the immunoreactive bands were visualized using the ECL+ kit. The immunoblots were quantified by measuring the density of each band with Image-J Software. The target protein expression was normalized to β-tubulin as a protein loading control.

Immunofluorescence

BV2 cells or PC-12 cells were fixed for 2 h at room temperature using 4% paraformaldehyde. After washing with PBS, cells needed to be permeabilized with 0.5% Triton X-100 for 10 min. Then, the frozen-sectioned brains and the permeabilized cells were washed with PBS and incubated with anti-Iba-1 or MAP2 antibody overnight in a wet chamber at 4 °C. Afterward, the brain tissues and the cells were washed with PBS, incubated with FITC-conjugated Donkey anti-Rabbit IgG in the dark for 1 h at 37°C. Next, the frozen-sectioned brains and the permeabilized cells were washed with PBS and incubated with anti-CD86, CD206, CREB, NGF, or β-Gal, GAP43 antibody overnight in a wet chamber at 4 °C. The brain tissues and the cells were washed with PBS, incubated with TRITC-conjugated Donkey anti-Rabbit IgG in the dark for 1 h at 37°C, followed by incubation with DAPI for 10 min at room temperature. Finally, immunofluorescence images were acquired by Confocal Laser Scanning Microscopy (C2, Nikon, Japan).

Enzyme-linked Immunoabsorbent Assay (ELISA)

The supernatants of BV2 cells were harvested. The blood of mice was collected from the eyeballs and centrifuged to collect serum. According to the manufacturer's protocol, the NGF, IL-1β, and IL-10 protein concentrations in BV2 cells and serum were determined by ELISA. Briefly, samples were assayed at 450 nm, and the concentrations were calculated from respective standard curves.

Flow Cytometric Analysis

BV2 cells were harvested by centrifuging after washing the BV2 cells with cold PBS. Next, BV2 cells were stained with anti-mouse CD86-FITC or anti-mouse CD206-APC followed standard protocols and manufacturer’s instructions. Finally, the stained cells were immediately analyzed by flow cytometry (BD, USA).

PC-12 cells were harvested and washed with cold PBS, followed by the addition of 195 μL binding buffers. Then incubate the cells with 5 μL Annexin V-FITC for 10 min and 10 μL PI for 5 min at room temperature in the dark. Finally, the stained cells were immediately analyzed by flow cytometry (BD, USA).

CCK-8 Assay

PC-12 cells with or without Aβ1-42 were cultured with the supernatant of different groups of BV2 cells in 96-well plates. Then, 10 μL CCK-8 reagents per well were added to the cells at 37°C for 2 h, and the absorbance at 450 nm was measured to calculate the cell viability using a multi-mode reader (LD942, Beijing, China).

Luciferase Reporter Assay

Plasmids of pcDNA3.1, pGL3, and CREBcDNA were constructed by Genewiz. The plasmid of the NGF promoter region containing five predicted sites to bind CREB would be constructed into WT and MUT plasmids. 293T cells and BV2 cells were seeded in 96-well plates. Then, according to the following group, to transfect the cells: pcDNA3.1 + pGL3, CREBcDNA + pGL3, CREBcDNA + NGF WT, CREBcDNA + NGF MUT. According to the manufacturer, transient transfection of plasmids into 293T cells and BV2 cells was performed using Lipofectamine 3000 transfection reagent's instructions (Invitrogen by Thermo Fisher Sci.). After 24 h post-transfection, cells were washed in PBS and lysed, and luminescence was measured following instructions of Nano-Glo ® Reporter Assay System Dual-Luciferase (Promega, USA).

Chromatin Immunoprecipitation (ChIP) Assay

ChIP assays were carried out according to the manufacturer's protocol (P2078, Beyotime Co.) with slight modifications. Chromatin solutions were sonicated and incubated with anti-CREB or with control IgG and rotated overnight at 4 °C. DNA-protein cross-links were reversed, and chromatin DNA was purified and subjected to PCR analysis. Forward and reverse primers were designed to amplify the NGF promoter region containing one predicted site to bind CREB to five predicted sites. After amplification, PCR products were resolved on a 2% agarose gel and visualized by ethidium bromide staining.

Senescence-associated β- Galactosidase Staining (SA-β-Gal)

Briefly, PC-12 cells in conditional culture were cultured in 6-well plates for 24 h, fixed with the fixative solution. Then senescence-associated β-galactosidase (SA-β-Gal) staining was performed according to the SA-β-Gal kit's instructions (Beyotime) for 12 h. The cells were then photographed under a microscope for the qualitative detection of SA-β-Gal activity.

GEO Analysis

Microarray datasets GSE48350 were downloaded from Gene Expression Omnibus and collected using the following platform: GPL570 [HG-U133 Plus 2]. The raw data was converted to a recognizable format by GEO2R. GEO2R performs comparisons on original submitter-supplied processed data tables using the GEOquery package, which parses GEO data into R data structures used by other R packages and limma (Linear Models for Microarray Analysis) R package from the Bioconductor project. Each chip group was compared with AD and NC, respectively. Difference analysis was performed by GEO2R analysis with $P < 0.05$ and log |FC| > 1 as the cutoff value for screening differentially expressed genes (DEGs). We used the

gplots R package to draw the heat map. Next, we calculated the Pearson correlation coefficients of related genes to calculate whether they were linearly related.

Statistical Analysis

All data were presented as mean ± standard deviation (SD). Differences between groups were assessed by one-way ANOVA, followed by Turkey's test using SPSS22.0. All assays were performed in triplicate. $P < 0.05$ was considered statistically significant.

Results

1. CCS improved learning and memory impairment and enhanced hippocampal neuronal synaptic plasticity in APP/PS1 mice

To explore the neuroprotective effect of CCS treatment, we used the Morris water maze, passive avoidance test, step-down test, and locomotivity test to investigate the learning and memory performance. After 4 weeks of intragastric administration of CCS, we used the Morris water maze test to study the effect of CCS treatment on the learning and memory capability of APP/PS1 mice. On the 1st day of the navigation test, there were no significant differences in escape latency and path length among all the groups (Figure 1A&B). From the 2nd to the 5th day, CCS treatment significantly shortened the escape latency (Figure 1A) and path length (Figure 1B) of APP/PS1 mice, compared with WT mice. On the 6th day of the probe trial, after removing the platform, we found that CCS treatment strikingly prolonged the time spending in the target quadrant (Figure 1C&D) and the frequencies of passing through the goal of APP/PS1 mice (Figure 1C&E). The results of the Morris water maze test suggested that CCS treatment improved learning and memory impairment in APP/PS1 mice.

To further confirm the efficacy of CCS treatment, we employed the passive avoidance test and step-down avoidance test. Consistent with the results of the Morris water maze test, CCS treatment significantly prolonged the latency (Figure 1F) and reduced the frequencies of entering the dark compartment (Figure 1G) of APP/PS1 mice in the passive avoidance test. And the step-down test also showed that CCS treatment increased the latency of the first jump (Figure 1H) and decreased the number of errors (Figure 1I) of APP/PS1 mice. The results further testified the anti-AD efficacy of CCS treatment.

In order to exclude the possible effect of locomotor activity on the behavioral test, we used the locomotivity test to investigate the locomotivity and the frequencies of stand-up among different groups. We found that there were no significant differences in the locomotivity and the frequencies of stand-up within 10 min among all the groups (Figure 1J&K). It was suggested that the changes in the behavioral tests were caused by the impairment of learning and memory, indeed, not affected by locomotivity. Therefore, the above results suggested that CCS treatment significantly ameliorated the cognitive deficits in spatial learning and memory of APP/PS1 mice.

Degeneration and senescence of neurons are closely related to the performance of learning and memory(19). We found that the expression of β-Gal was increased in the hippocampus of APP/PS1 mice, while it was decreased after CCS treatment (Figure 1L&M). It was suggested that CCS treatment improved the senescence in the hippocampus of APP/PS1 mice. As the senescence correlated with neuronal plasticity(20), we further investigated the expression levels of neuronal markers and plasticity-related proteins. As expected, after CCS treatment, the expressions of neuronal markers including MAP2 and NeuN were increased, and simultaneously the synaptic protein expressions such as GAP43 and Syn were also elevated in the hippocampus of APP/PS1 mice, compared with the APP/PS1 group (Figure 1N&O). Besides, we investigated the efficacy of CCS treatment by Transmission Electron Microscopy (TEM). It was found that the intact synapse structures, including synaptic vesicles, presynaptic and postsynaptic membrane, synaptic spaces, and dense postsynaptic zones, could be clearly observed in the hippocampus of the WT group. However, in APP/PS1 group, the synaptic structure was incomplete, the synaptic vesicles were decreased, the boundary between the presynaptic and postsynaptic membrane was unclear, the synaptic space was blurred, and the density of the dense postsynaptic zone was decreased. CCS treatment effectively improved the synaptic morphology of neurons, made the synaptic structure intact, and increased the density of the dense postsynaptic zone in the hippocampus of APP/PS1 mice, indicating that CCS treatment promoted the synaptic remodeling (Figure 1P). In a word, CCS improved learning and memory impairment by ameliorating senescence and enhancing neuronal plasticity in APP/PS1 mice.

2. CCS promoted microglial M2 polarization to improve the microenvironment, possibly attributed to NGF upregulation

Microglia (MG) is an important component of the neuronal microenvironment. Different microglial polarization status will significantly affect the neuroimmune microenvironment and finally decided the destiny of neurons(21). Therefore, we analyzed the differential expression of the GSE48350 chip in the GEO database, including the samples of 48 normal elderly and 21 AD patients. We found that the expression of M1 marker TNF in AD patients was increased compared with those of normal elderly, while the expression of M2 marker Arg1 was decreased (Figure 2A&B). It was suggested that MG-M1/M2 phenotypic transformation played an important role in the occurrence and development of AD. However, whether CCS treatment could improve the neuronal microenvironment by regulating the MG-M1/M2 phenotypic transformation has not been reported until now. To further investigate the effects of CCS treatment on the MG-M1/M2 phenotypic transformation, we also examined the expressions of M1 and M2 phenotypic markers in the hippocampus of APP/PS1 mice treated with CCS. Consistent with the result of GEO analysis, it was found that the expressions of M1 phenotypic markers IL-1β, TNF-α, and iNOS were significantly increased, and the expressions of M2 phenotypic markers IL-10, TGF-β, and Arg1 were decreased in the hippocampus of APP/PS1 mice (Figure 2C), compared with the WT group. After CCS treatment, we gladly found that the expressions of M1 markers were significantly decreased, while the expressions of M2 markers were increased (Figure 2C), compared with the APP/PS1 group. Immunofluorescence staining indicated that Iba-1 co-localized with CD86 or CD206, CCS decreased the expression of Iba-1 and CD86, and increased CD206 expression in the hippocampus of APP/PS1 mice

(Figure 2D&E). Furthermore, ELISA results showed that the IL-1β secretion was inhibited, and the IL-10 secretion was elevated in the peripheral blood of APP/PS1 mice after CCS treatment (Figure 2F&G). These results suggested that CCS treatment improved the neuroimmune microenvironment after microglial M2 polarization in the hippocampus of APP/PS1 mice.

Next, we were interested in the major effector improving the neuroimmune microenvironment after microglial M2 polarization. Our previous study reported that NGF in the hippocampus of APP/PS1 mice was deficient, and drug treatment significantly reduced Aβ deposition and improved the learning and memory impairments(9). Accordingly, NGF expression in AD patients was also lower than the normal elderly in GSE48350 (Figure 2H-I). Therefore, we suspected whether NGF was the effector correlated with microglial M2 polarization. Pearson correlation analysis showed that there was a positive correlation between NGF and M2 phenotypic marker Arg1 (Figure 2J), but there was no correlation between NGF and M1 phenotypic marker TNF (Figure 2J), indicating that NGF might be the key effector associated with microglial M2 polarization and had an influence on the neuroimmune microenvironment. Then, we verified the expression and secretion of NGF in the hippocampus and the peripheral blood. Compared with the WT group, the expression and secretion of NGF in the hippocampus and the peripheral blood of APP/PS1 mice were decreased. And the expression and secretion of NGF were increased after CCS treatment (Figure 2K-M). Therefore, NGF might be the major effector to improve the microenvironment by microglial M2 polarization after CCS treatment.

Furthermore, we investigated the efficacy of CCS treatment in BV2 cells treated with/without LPS+IFNγ to testify the results in vivo. First, we induced microglial M1 polarization by LPS+IFNγ and then treated it with different CCS concentrations. As expected, the expressions of M1 phenotypic markers IL-1β, TNF-α, and iNOS were decreased after CCS treatment; in contrast, the expressions of M2 phenotypic markers IL-10, TGF-β, and Arg1 were increased (Figure 3A-D), following a concentration-dependent manner. The results of Flow Cytometry and Immunofluorescence staining noted that CCS inhibited the expression of M1 phenotypic marker CD86 and increased the expression of M2 phenotypic marker CD206 in LPS+IFNγ-treated BV2 cells (Figure 3E-H). It showed that CCS treatment made M1 phenotype (MG-M1) polarized to M2 phenotype microglia (MG-M2). Surprisingly, we found that 1 μg/mL CCS itself also decreased the expressions of M1 markers and enhanced the expressions of M2 markers in untreated BV2 cells (Figure 3A-H), indicating that CCS could promote MG-M2 polarization, not only from MG-M1 but also from resting status (MG-M0). Simultaneously, we also determined the mRNA, protein, and secretion levels of NGF. Immunofluorescence staining indicated that NGF was co-located with Iba-1, a marker of MG activation, and CCS treatment increased the low expression of NGF in the LPS+IFNγ group (Figure 3I). The results of qPCR and RT-PCR showed that CCS treatment increased the mRNA level of NGF in a concentration-dependent manner; meanwhile, it also induced microglial M2 polarization (Figure 3J&K), which was consistent with the results of protein expression and secretion level of NGF (Figure 3L&M). The above results suggested that CCS promoted microglial M2 polarization to improve the microenvironment of neurons, and NGF might be the major effector contributing to this procession.

3. MG-derived NGF was the pivotal factor in the neuronal microenvironment to improve the Aβ1-42-induced neuronal senescence and plasticity after CCS-induced MG-M2 polarization

To further clarify the key role of MG-derived NGF in CCS-induced microglial M2 polarization on neuronal function, we used Aβ1-42-induced PC-12 cells for conditional culture. AD neurons were cultured in the supernatant medium of BV2 cells treated with different treatments (Figure 4A). The conditional medium of LPS+IFNγ-induced BV2 cells (M1-CM) significantly reduced the cell viability of AD neurons (Figure 4C) and elevated the cell apoptosis rate (Figure 4D). And the expression of β-Gal, an index related to senescence, was significantly increased (Figure 4E-G). Expressions of synaptic plasticity-related proteins such as GAP43 and Syn and those of neuronal markers such as MAP2 and NeuN were decreased strikingly (Figure 4F&H). It was suggested that the M1-CM exacerbated the neuron-microenvironment and dramatically affected the destiny of neurons. It was not surprising that M1-CM after CCS treatment markedly improved the cell viability of AD neurons (Figure 4C), inhibited neuronal apoptosis (Figure 4D), reduced the β-Gal expression (Figure 4E-G), and increased the expressions of GAP43, Syn, MAP2, and NeuN significantly (Figure 4F&H). This suggested that CCS treatment improved the neuroimmune microenvironment to affect neurons' fate by promoting microglial M2 polarization. However, is NGF the pivotal effector in this procession? To further clarify the crucial role of NGF in the symphony between microglia and neurons after CCS treatment, rNGF was added into MG-M1 to rescue the harmful effects, and anti-NGF was used to antagonize the beneficial effects of CCS on MG-M1. Fortunately, we found that the exogenous rNGF recovered the decreased neuronal apoptosis, senescence, and synaptic plasticity induced by the conditional medium of MG-M1 (M1-CM); moreover, the beneficial effects of CCS on AD neurons were antagonized by anti-NGF in the CCS-treated M1-CM (Figure 4C-H). There was no significant difference between the anti-NGF group and the LPS+IFNγ-induced BV2 cells group. It indirectly suggested that it was NGF secreted from MG-M2 induced by CCS to elicit the major beneficial support for AD neurons. Therefore, we demonstrated that CCS promoted microglial M2 polarization and then increased the MG-derived NGF to play a pivotal role in improving the neuroimmune microenvironment and regulating the function of AD neurons.

4. CCS treatment increased NGF levels after inducing microglial M2 polarization attributed to CREB activation

We revealed that CCS treatment increased NGF expression via promoting microglial M2 polarization; however, the regulation mechanism still remains unclear. Literature had shown that anti-inflammatory treatment with epilepsy and epilepsy-associated depression could cause a high expression of CREB, which affected neuronal loss(22). And CREB is also a regulatory factor initiating the transcription of BDNF, which was another major factor in the neurotrophic factor family(23). Therefore, we speculated whether CREB might regulate the transcription of NGF after CCS treatment. In vivo study showed that NGF expression was decreased in the hippocampus of APP/PS1 mice, and at the same time, the expressions of CREB and phosphorylated CREB (pCREB) were significantly decreased. CCS treatment not only elevated NGF expressions by inducing microglial M2 polarization but also increased the expressions of CREB and pCREB by Western Blotting (Figure 5A) and Immunofluorescence staining (Figure 5B&C).

Further, we also validated the results in vitro. The results showed that CCS treatment increased the expressions of CREB and pCREB in LPS+IFNγ-induced BV2 cells in a concentration-dependent manner by Western Blotting (Figure 5D), in accordance with the consequences of Immunofluorescence staining (Figure 5E&F). KG501, a specific inhibitor of CREB(24), was utilized to testify whether CREB activation participated in NGF regulation. CREB inactivation by KG501 could block the mRNA and protein expression and secretion of NGF in CCS-treated MG-M1(Figure 5G-J). It was prompted that CREB was the key regulator for NGF up-regulation in the procession of CCS-induced microglial M2 polarization.

5. CREB bound with the key binding site *sg3* (-1018~-1011) of the NGF promoter to promote NGF transcription to mediate the neuronal plasticity

We discovered that CREB activation regulated the mRNA level, protein expression, and secretion of NGF. Previous studies had demonstrated that CREB, as a transcription factor, could regulate the expressions of downstream genes. Therefore, we assumed CREB might regulate NGF in a transcriptional manner. We obtained the prediction results on the JASPAR online biological prediction website. It was found that CREB could bind with the NGF promoter region through *sg1* (-1381~-1374), *sg2* (-1135~-1128), *sg3* (-1018~-1011), *sg4* (-425~-418), and *sg5* (-218~-211) shown in Figure 6A. According to the predicted results, we constructed a plasmid containing luciferase reporter gene of NGF promoter sequence, which contains the wild type (WT) and full-length mutant (MUT) with 5 sites of predicted binding of CREB with NGF promoter region. The results of Luciferase Reporter Assay showed that the luciferase activity of double-transfected *CREBcDNA* with full-length NGF mutant plasmid (MUT) was remarkedly lower than that of WT plasmid (Figure 6B) in 293T and BV2 cells, suggesting that CREB could bind with NGF promoter region indeed. ChIP results revealed that CREB actually bound with the promoter region of NGF (Figure 6C). To find out the exact key binding sites between CREB and NGF promoter regions, we designed the primer sequences of the five CRE binding sites (*sg1*~*sg5*) for ChIP Assay. It was noted that CREB could bind with *sg3* in the promoter region of NGF (Figure 6D). For further confirmation, we constructed a plasmid containing wild type and mutant luciferase reporter genes of *sg3* in the NGF promoter sequence. After the *sg3* mutation, the luciferase activity of the *sg3*-MUT group was reduced (Figure 6E) compared with the *sg3*-WT group. It was further confirmed that *sg3* was the key binding site for CREB and NGF promotor. In order to investigate the expression and secretion levels of NGF, we transfected *sg3*-WT or *sg3*-MUT plasmid in BV2 cells with *CREBcDNA* double-transfection. We discovered that after CREB overexpression, the mRNA level, protein expression, and secretion were all dramatically decreased in the *sg3*-MUT group, compared with those in the *sg3*-WT group (Figure 6F-I). It was proved that CREB could bind with the *sg3* binding site (-1018~-1011) in the promoter region of NGF, initiate NGF transcription, and then up-regulate the expression and secretion of NGF in BV2 cells.

As mentioned above, since CREB regulated the NGF expression by directly binding with *sg3* in the promoter region of NGF, we further studied the effects on AD neurons after different CM transfected with sg3-WT or sg3-MUT plasmid (Figure 7A). CREB-overexpressed CM treated with *sg3*-WT significantly increased the cell viability of AD neurons (Figure 7B), reduced the apoptosis rate and β-Gal expression (Figure 7C-E), and increased the expressions of GAP43, Syn, MAP2, and NeuN (Figure 7D&F). However,

when *sg3* was mutant, CREB could not bind with the NGF promoter anymore, the expression and secretion levels of NGF were significantly lower in the *sg3*-MUT group than those in the *sg3*-WT group, and the beneficial effects of NGF above dramatically vanished. It was further indicated that CREB effectively bound with the promoter region of NGF in BV2 cells, up-regulated the expression and secretion of NGF, and then reduced the cell apoptosis and senescence of AD neurons, produced the neuronal remodeling.

Above all, we concluded that CCS treatment activated CREB driven by microglia M2 polarization, induced the CREB bound with *sg3* site (-1018~-1011) in the NGF promoter region, and then up-regulated NGF expression and secretion to improve the microenvironment of AD neurons, and finally led to neuroprotective incomes.

Discussion

MG, as resident macrophage-like immune cells in the central nervous system (CNS), is scattered around neurons and continuously senses the micro changes of the surrounding environment by structural support, neuro-nutrition, and immune surveillance(25). There were two major phenotypes after MG activation and one is MG-M1, the other is MG-M2. MG-M1 is characterized by the secretion of inflammatory factors such as IL-1β, TNF-α, etc. In contrast, MG-M2, an "alternative activation", induces the secretion of anti-inflammatory factors such as TGF-β, Arg1 and also increases the expressions of neurotrophic factors to amend the aggravating microenvironment to sustain the normal neuronal function(26). In AD, MG was excessively activated and polarized to MG-M1 from resting status, leading to Aβ deposition, abnormal tau accumulation, neuronal damage, and synaptic dysfunction(26, 27). Therefore, the phenotypes of MG polarization will largely affect the symphony between MG and neurons and decide AD neurons' final fate. It is an effective way to fight against AD by finding out potential compounds improving the MG-mediated microenvironment.

Fortunately, we discovered an anti-AD compound named Cordycepin (CCS) isolated from *Cordyceps militaris.* It was reported about its health-promoting properties, including anti-inflammatory, antioxidant, anti-tumor, and immunomodulatory functions(28). However, there was no report on whether CCS had anti-AD efficacy and whether CCS might have promoted MG-M2 polarization to orchestrate the symphony between MG and neurons. We found that CCS treatment improved the cognitive impairment in APP/PS1 mice and inhibited excessive MG activation. CCS also induced the MG-M2 polarization by increasing the levels of M2 markers and decreasing the expressions of M1 markers. This is consistent with the anti-inflammatory effects of CCS in some reports(15). Also, this was the first report about the CCS-induced MG-M2 polarization from resting status. Furthermore, we also found that the senescence and synaptic damage of hippocampal neurons were also effectively improved with CCS treatment in vivo and in vitro. It was indicated that CCS was actually a potential compound targeting MG-mediated microenvironment, not only for AD therapy but also for keeping good health in the normal elderly population.

Since CCS could modulate the microglial polarization, we tried to determine an effector orchestrating the symphony between microglia and neurons in this procession. In the GEO database, we discovered that NGF was significantly decreased in AD patients. NGF, as a member of the neurotrophic factor family, has powerful effects on neuronal nurturing(29). Our previous study had reported that NGF deficiency occurred in the hippocampus of APP/PS1 mice, leading to cognitive deficits(9). Some studies also found that NGF could effectively reverse the inflammation in Aβ-induced MG to elicit the effects of anti-inflammation and neuroprotection(30). Encouragingly, we also found that it was positively correlated with Arg1, an MG-M2 marker in AD patients. And both in vivo and in vitro studies showed that the NGF level was also elevated following MG-M2 polarization after CCS treatment. As we expected, CCS also recovered the senescence and synaptic damage of AD neurons in vivo and in vitro by conditional culture with M1-CM. Exogeneous rNGF improved the harmful effects on neurons caused by M1-CM, while the beneficial response to CCS-treated CM would be neutralized after NGF antagonism by anti-NGF, which indicated that MG-derived NGF might be the target effector to orchestrate the communication between MG and neurons in CCS-mediated anti-AD efficacy.

CREB activation was found to be associated with NGF expression after CCS treatment in our study. It was also reported that dopamine treatment caused BDNF up-regulation mediating by exons IV and VI in the distal regulatory elements of BDNF via the cAMP/CREB signal pathway(31). Mohammadi et al. summarized that BDNF up-regulated the related genes downstream via CREB, including the genes in PI3K/AKT, PLC-γ, and MAPK/ERK signal pathway(32). However, there is no literature about the relationship between NGF and CREB and the regulatory mechanism. In order to explore the regulatory relationship between CREB and NGF in MG, we used JASPAR online biological prediction to find whether CREB could bind with five sites *sg1~sg5* in the promoter region of NGF. We firstly discovered *sg3* (-1018~-1011 site) in the promoter region of NGF was the key binding site of CREB. As a result, CCS induced MG-M2 polarization, activated CREB, promoted NGF transcription, increased the expression and secretion of NGF, orchestrated with AD neurons, and finally improved the senescence, apoptosis, and synaptic remodeling.

Conclusion

In a word, we found that the neuroinflammatory microenvironment targeting MG-M2 polarization was a novel pointcut for both AD therapy and anti-AD new drug development. Based on the view, we found a potential compound, CCS, which could promote MG-M2 polarization from both M1 and resting status. It was MG-derived NGF orchestrating the symphony communication between microglia and neurons and deciding the neurons' destiny after CCS treatment. Additionally, we also discovered a new regulatory mechanism of CCS to improve the neuronal functions: CREB-involved NGF transcription by direct binding with *sg3* (-1018~-1011 site) in the promoter region of NGF. These findings show a possible effector in the microenvironment of AD neurons and provide a new strategy for further clinical interventions of AD.

Abbreviations

Aβ: Amyloid β; AD: Alzheimer's disease; APP: Amyloid Precursor Protein; Arg1: Arginase-1; β-Gal: β-Galactosidase; CCS: Cordycepin; CREB: cAMP-response element binding protein; GAP43: Growth associated protein-43; IFNγ: Interferon-γ; IL-1β: Interleukin-1β; IL-10: Interleukin-10; iNOS: inducible Nitricoxide Synthetase; LPS: Lipopolysaccharide; MG: Microglia; NGF: Nerve Growth Factor; PS: Presenilin; Syn: Synaptophysin; TNF-α: Tumor Necrosis Factor-α; TGF-β: Transforming growth factor-β.

Declarations

Ethics approval and consent to participate

All animal care and experimental procedures were in line with the Laboratory Animal Ethical Standards of China Medical University and the Standard Medical Laboratory Animals' Care and Use Protocols.

Consent for publication

All authors have given their consent for publication.

Availability of data and materials

Data sharing not applicable to this article as no datasets were generated or analyzed during the current study.

Competing interests

The authors have declared that no competing interest exists.

Fundings

This work was supported by the National Natural Science Foundation of China (No. 81501098, 81603122, 81901309), Major Special S&T Projects in Liaoning Province [2019JH1/10300005], Shenyang S&T Project (20-204-4-22), The Drug Innovation Major Project of National High Technology Research and Development Program of China (2018ZX09711001-008-006), Key R&D Plan Guidance Project of Liaoning Province (No.2018225089, ZF2019037), Doctoral Research Startup Fund Project of Liaoning Province (2019-BS-289).

Authors' contributions

Linchi Jiao, Mingyan Liu, and Minjie Wei designed and conceived the research. Linchi Jiao, Xin Zhong, Ke Du, Yuqiang Wu, and Jia Fu performed cell experiments. Linchi Jiao, Weifan Yao, Jiajia Shen, Junxiu Liu, and Junhui Tong conducted the animal experiments. Linchi Jiao and Guowei Ma performed the constructions of plasmids. Linchi Jiao, Jiajia Shen, and Chao Liu analyzed the data in GEO. Linchi Jiao, Mingyan Liu, and Minjie Wei collected and analyzed the data. Linchi Jiao, Mingyan Liu, Zhihua Yu, and Minjie Wei wrote and revised the manuscript. All authors approved the final manuscript.

References

1. Hansen DV, Hanson JE, Sheng M. Microglia in Alzheimer's disease. The Journal of cell biology. 2018;217(2):459-72.
2. Uchoa MF, Moser VA, Pike CJ. Interactions between inflammation, sex steroids, and Alzheimer's disease risk factors. Frontiers in neuroendocrinology. 2016;43:60-82.
3. Heppner FL, Ransohoff RM, Becher B. Immune attack: the role of inflammation in Alzheimer disease. Nature reviews Neuroscience. 2015;16(6):358-72.
4. Hammond TR, Marsh SE, Stevens B. Immune Signaling in Neurodegeneration. Immunity. 2019;50(4):955-74.
5. Shi Y, Holtzman DM. Interplay between innate immunity and Alzheimer disease: APOE and TREM2 in the spotlight. Nature reviews Immunology. 2018;18(12):759-72.
6. Heneka MT, Carson MJ, El Khoury J, Landreth GE, Brosseron F, Feinstein DL, et al. Neuroinflammation in Alzheimer's disease. The Lancet Neurology. 2015;14(4):388-405.
7. Tuszynski MH, Yang JH, Barba D, U HS, Bakay RA, Pay MM, et al. Nerve Growth Factor Gene Therapy: Activation of Neuronal Responses in Alzheimer Disease. JAMA neurology. 2015;72(10):1139-47.
8. Chen XQ, Mobley WC. Exploring the Pathogenesis of Alzheimer Disease in Basal Forebrain Cholinergic Neurons: Converging Insights From Alternative Hypotheses. Frontiers in neuroscience. 2019;13:446.
9. Liu M, Chen F, Sha L, Wang S, Tao L, Yao L, et al. (-)-Epigallocatechin-3-gallate ameliorates learning and memory deficits by adjusting the balance of TrkA/p75NTR signaling in APP/PS1 transgenic mice. Molecular neurobiology. 2014;49(3):1350-63.
10. Zhong X, Liu M, Yao W, Du K, He M, Jin X, et al. Epigallocatechin-3-Gallate Attenuates Microglial Inflammation and Neurotoxicity by Suppressing the Activation of Canonical and Noncanonical Inflammasome via TLR4/NF-κB Pathway. Molecular nutrition & food research. 2019;63(21):e1801230.
11. Tuli HS, Sharma AK, Sandhu SS, Kashyap D. Cordycepin: a bioactive metabolite with therapeutic potential. Life sciences. 2013;93(23):863-9.
12. Yoon SY, Park SJ, Park YJ. The Anticancer Properties of Cordycepin and Their Underlying Mechanisms. International journal of molecular sciences. 2018;19(10).
13. Choi YH, Kim GY, Lee HH. Anti-inflammatory effects of cordycepin in lipopolysaccharide-stimulated RAW 264.7 macrophages through Toll-like receptor 4-mediated suppression of mitogen-activated protein kinases and NF-κB signaling pathways. Drug design, development and therapy. 2014;8:1941-53.
14. An Y, Li Y, Wang X, Chen Z, Xu H, Wu L, et al. Cordycepin reduces weight through regulating gut microbiota in high-fat diet-induced obese rats. Lipids in health and disease. 2018;17(1):276.
15. Jeong JW, Jin CY, Kim GY, Lee JD, Park C, Kim GD, et al. Anti-inflammatory effects of cordycepin via suppression of inflammatory mediators in BV2 microglial cells. International immunopharmacology.

2010;10(12):1580-6.
16. Cheng Z, He W, Zhou X, Lv Q, Xu X, Yang S, et al. Cordycepin protects against cerebral ischemia/reperfusion injury in vivo and in vitro. European journal of pharmacology. 2011;664(1-3):20-8.
17. Jin ML, Park SY, Kim YH, Oh JI, Lee SJ, Park G. The neuroprotective effects of cordycepin inhibit glutamate-induced oxidative and ER stress-associated apoptosis in hippocampal HT22 cells. Neurotoxicology. 2014;41:102-11.
18. Cai ZL, Wang CY, Jiang ZJ, Li HH, Liu WX, Gong LW, et al. Effects of cordycepin on Y-maze learning task in mice. European journal of pharmacology. 2013;714(1-3):249-53.
19. Liu B, Liu W, Liu P, Liu X, Song X, Hayashi T, et al. Silibinin Alleviates the Learning and Memory Defects in Overtrained Rats Accompanying Reduced Neuronal Apoptosis and Senescence. Neurochemical research. 2019;44(8):1818-29.
20. Smith GS. Aging and neuroplasticity. Dialogues in clinical neuroscience. 2013;15(1):3-5.
21. L'Episcopo F, Tirolo C, Serapide MF, Caniglia S, Testa N, Leggio L, et al. Microglia Polarization, Gene-Environment Interactions and Wnt/β-Catenin Signaling: Emerging Roles of Glia-Neuron and Glia-Stem/Neuroprogenitor Crosstalk for Dopaminergic Neurorestoration in Aged Parkinsonian Brain. Frontiers in aging neuroscience. 2018;10:12.
22. Shen Y, Peng W, Chen Q, Hammock BD, Liu J, Li D, et al. Anti-inflammatory treatment with a soluble epoxide hydrolase inhibitor attenuates seizures and epilepsy-associated depression in the LiCl-pilocarpine post-status epilepticus rat model. Brain, behavior, and immunity. 2019;81:535-44.
23. Jiang B, Wang H, Wang JL, Wang YJ, Zhu Q, Wang CN, et al. Hippocampal Salt-Inducible Kinase 2 Plays a Role in Depression via the CREB-Regulated Transcription Coactivator 1-cAMP Response Element Binding-Brain-Derived Neurotrophic Factor Pathway. Biological psychiatry. 2019;85(8):650-66.
24. Wu HY, Tang XQ, Liu H, Mao XF, Wang YX. Both classic Gs-cAMP/PKA/CREB and alternative Gs-cAMP/PKA/p38β/CREB signal pathways mediate exenatide-stimulated expression of M2 microglial markers. Journal of neuroimmunology. 2018;316:17-22.
25. Hickman S, Izzy S, Sen P, Morsett L, El Khoury J. Microglia in neurodegeneration. Nature neuroscience. 2018;21(10):1359-69.
26. Sarlus H, Heneka MT. Microglia in Alzheimer's disease. The Journal of clinical investigation. 2017;127(9):3240-9.
27. Heneka MT, Kummer MP, Stutz A, Delekate A, Schwartz S, Vieira-Saecker A, et al. NLRP3 is activated in Alzheimer's disease and contributes to pathology in APP/PS1 mice. Nature. 2013;493(7434):674-8.
28. Yuan J, Wang A, He Y, Si Z, Xu S, Zhang S, et al. Cordycepin attenuates traumatic brain injury-induced impairments of blood-brain barrier integrity in rats. Brain research bulletin. 2016;127:171-6.
29. Ding XW, Li R, Geetha T, Tao YX, Babu JR. Nerve growth factor in metabolic complications and Alzheimer's disease: Physiology and therapeutic potential. Biochimica et biophysica acta Molecular

basis of disease. 2020;1866(10):165858.
30. Rizzi C, Tiberi A, Giustizieri M, Marrone MC, Gobbo F, Carucci NM, et al. NGF steers microglia toward a neuroprotective phenotype. Glia. 2018;66(7):1395-416.
31. Koppel I, Jaanson K, Klasche A, Tuvikene J, Tiirik T, Pärn A, et al. Dopamine cross-reacts with adrenoreceptors in cortical astrocytes to induce BDNF expression, CREB signaling and morphological transformation. Glia. 2018;66(1):206-16.
32. Mohammadi A, Amooeian VG, Rashidi E. Dysfunction in Brain-Derived Neurotrophic Factor Signaling Pathway and Susceptibility to Schizophrenia, Parkinson's and Alzheimer's Diseases. Current gene therapy. 2018;18(1):45-63.

Figures

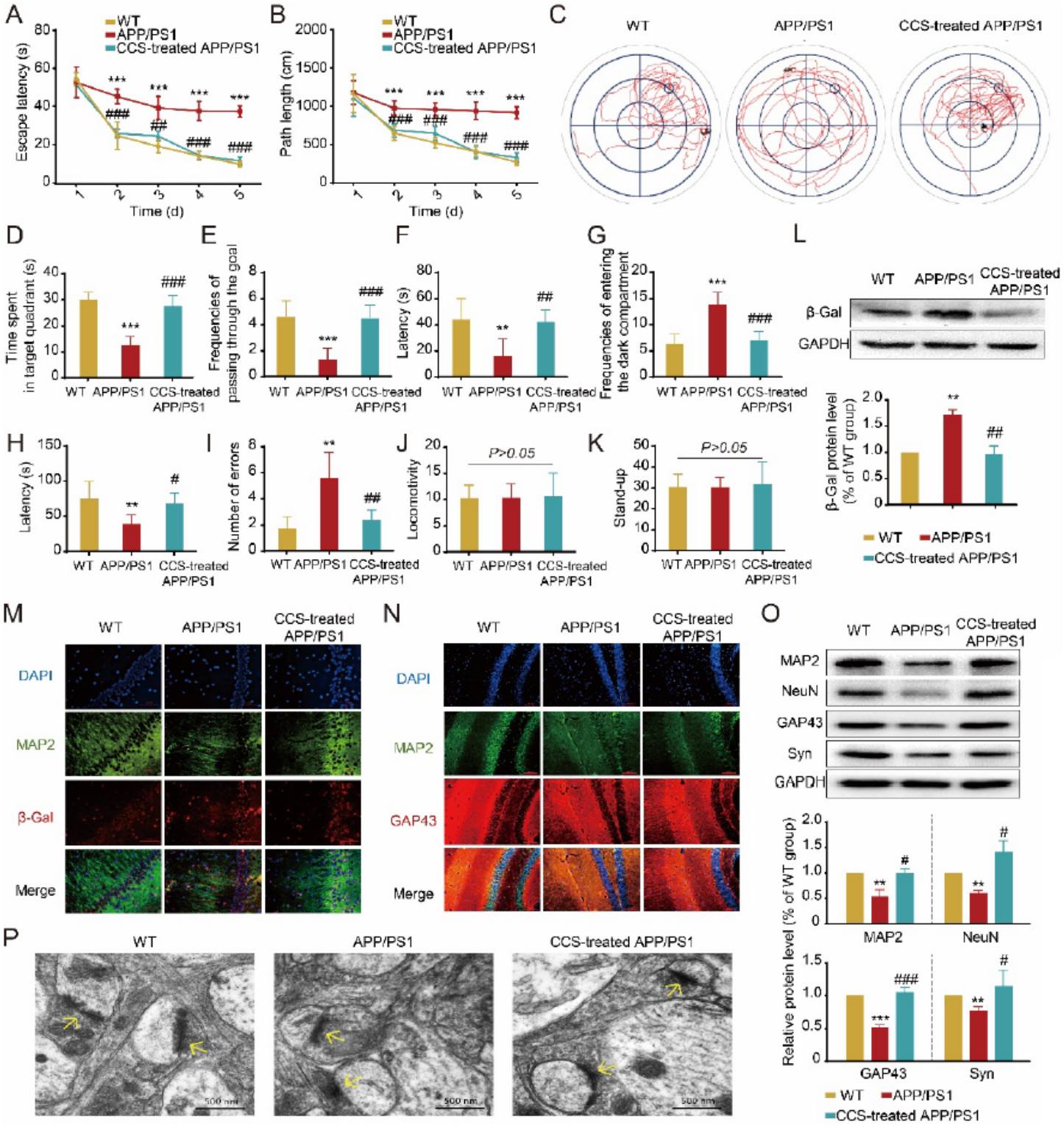

Figure 1

CCS improved learning and memory impairment and enhanced hippocampal neuronal synaptic plasticity in APP/PS1 mice. The escape latency (A) and the path length (B) of APP/PS1 mice treated with CCS were investigated in the navigation test of the Morris water maze. The presentative tracing figures of APP/PS1 mice treated with CCS in the probe trial (C). The time spent in the target quadrant (D) and the frequencies of passing through the goal (E) of APP/PS1 mice treated with CCS were investigated in the probe trial of

the Morris water maze. The latency (F) and the frequencies of entering the dark compartment (G) of APP/PS1 mice treated with CCS were investigated in the passive avoidance test. The latency (H) and the number of errors (I) of APP/PS1 mice treated with CCS were investigated by the step-down avoidance test. CCS treatment did not affect locomotivity (J) and the frequencies of stand-up (K) of APP/PS1 mice in the locomotivity test. The expression of β-Gal in the hippocampus of APP/PS1 mice after CCS treatment was measured by Western Blotting (L) and Immunofluorescence (M). The expression of neuronal synaptic protein GAP43 in the hippocampus of APP/PS1 mice after CCS treatment was measured by Immunofluorescence (N). The expressions of MAP2, NeuN, GAP43, and Syn in the hippocampus of APP/PS1 mice after CCS treatment were measured by Western Blotting (O). CCS treatment improved the hippocampus's neuronal synaptic ultrastructure in APP/PS1 mice by Transmission Electron Microscopy (P). Arrows showed the characteristic changes of neuronal synapse in the hippocampus of APP/PS1 mice. *P<0.05, **P<0.01, ***P<0.001, compared with WT group; #P<0.05, ##P<0.01, ###P<0.001, compared with APP/PS1 group.

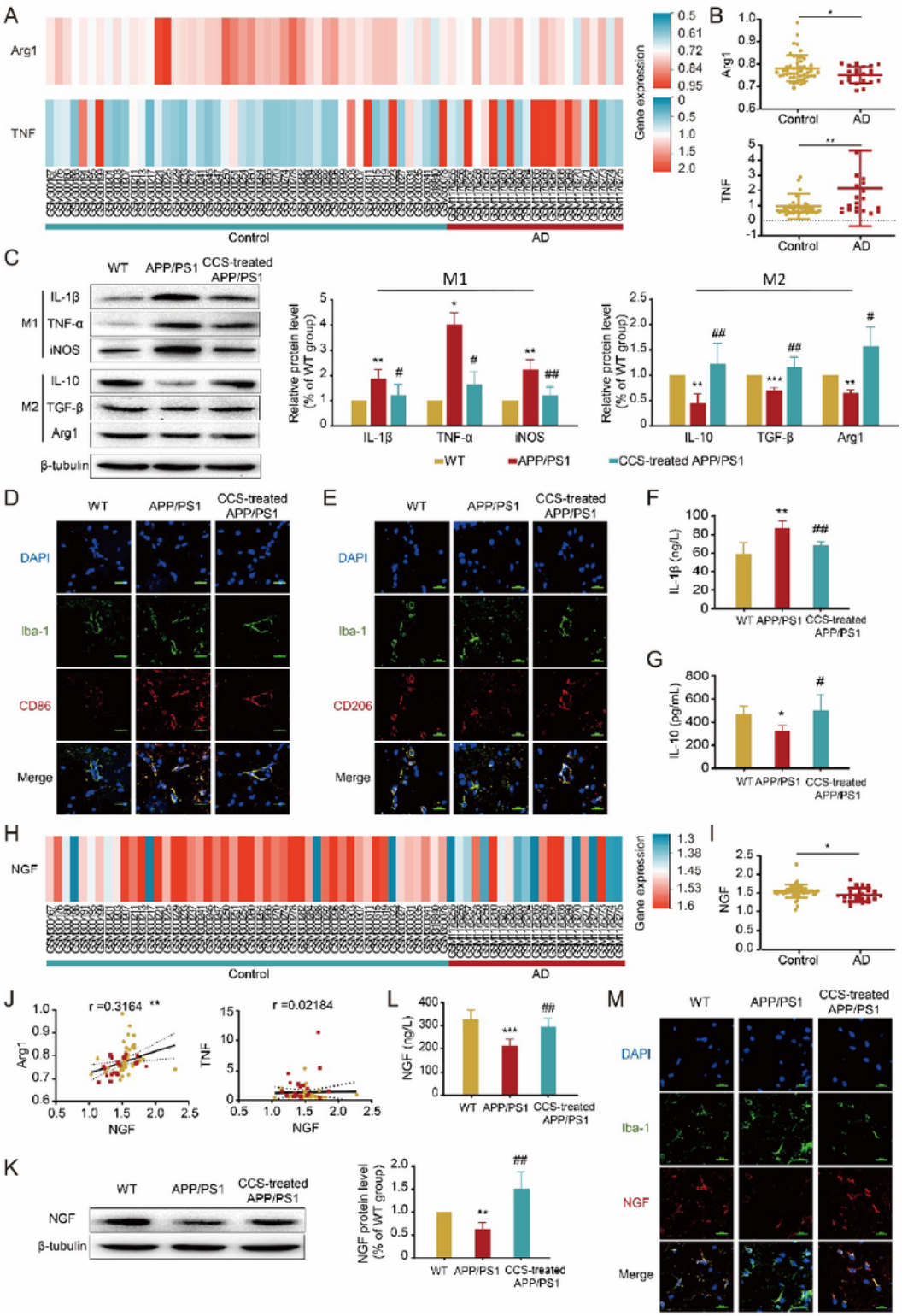

Figure 2

CCS promoted microglial M2 polarization to improve the microenvironment, possibly attributed to NGF upregulation. GSE48350 microarray chip revealed the differential gene expression of Arg1 and TNF genes in the normal elderly and AD patients (A). The expression of Arg1 was significantly decreased, while the expression of TNF was increased (B) in AD patients. The expression levels of the M1 phenotype markers IL-1β, TNF-α, iNOS, and M2 phenotype markers IL-10, TGF-β, and Arg1 in the hippocampus of APP/PS1

mice after CCS treatment were detected by Western Blotting (C). The co-localizations and expressions of microglial marker Iba-1 with CD86 (D) or CD206 (E) in the hippocampus of APP/PS1 mice after CCS treatment were examined by Immunofluorescence. The secretions of IL-1β (F) and IL-10 (G) in the peripheral blood of APP/PS1 mice after CCS treatment were measured by ELISA. The NGF gene's heatmap in the normal elderly and AD patients by GSE48350 microarray chip (H). The expression of NGF was significantly decreased in AD patients (I). The NGF was significantly correlated with Arg1; however, there was no relationship between NGF and TNF by Pearson correlation analysis (J). The expression and secretion of NGF were both increased in the hippocampus of APP/PS1 mice after CCS treatment by Western Blotting (K), ELISA (L), and Immunofluorescence (M). *P<0.05, **P<0.01, ***P<0.001, compared with WT group; #P<0.05, ##P<0.01, ###P<0.001, compared with APP/PS1 group.

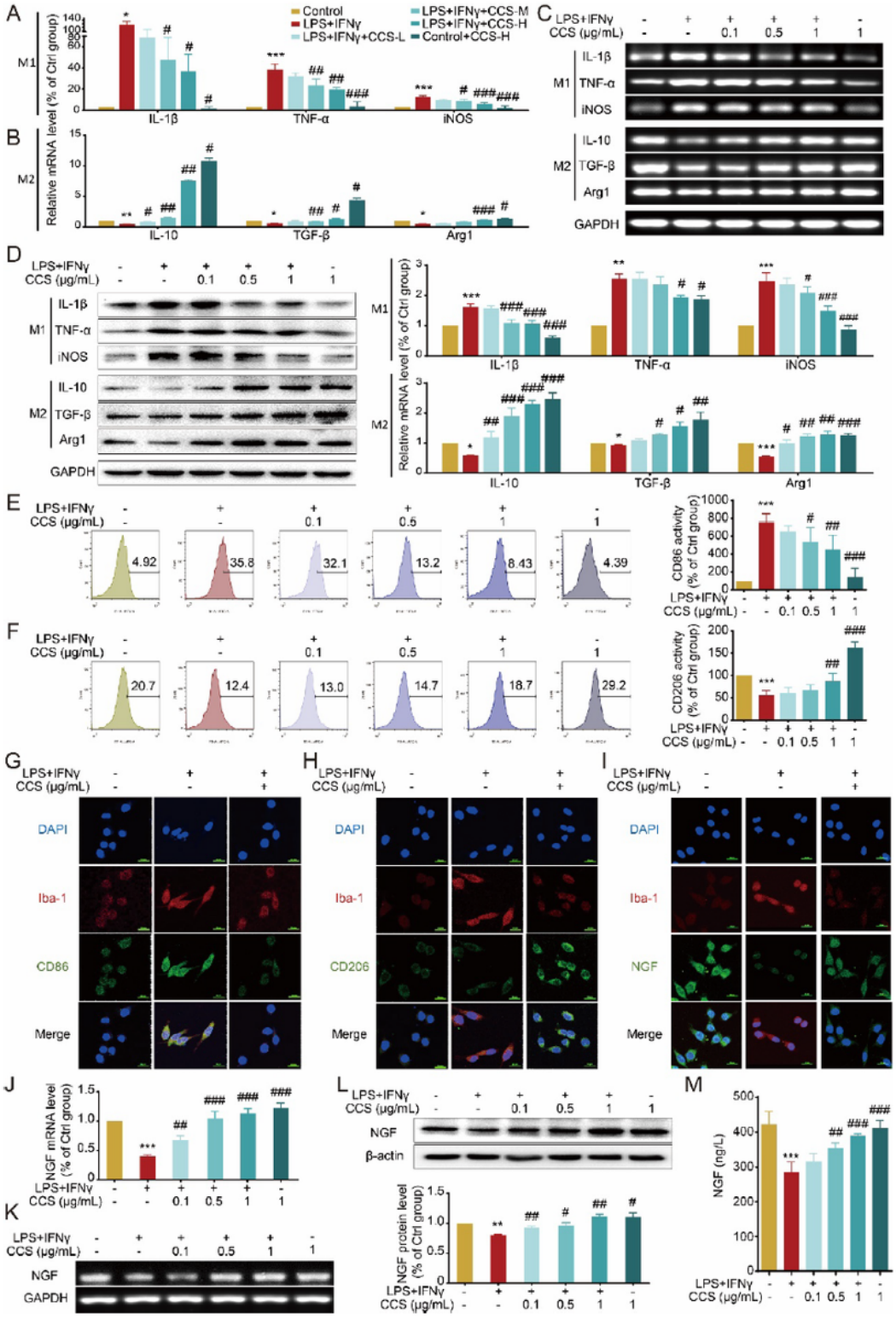

Figure 3

CCS not only promoted the LPS+IFNγ-induced MG-M1 to MG-M2 but also induced MG-M0 polarized to MG-M2, leading to the ensued upregulation of NGF in BV2 cells. The transcription levels of M1 phenotype markers IL-1β, TNF-α, iNOS (A), and M2 phenotype markers IL-10, TGF-β, Arg1 (B) in LPS+IFNγ-induced BV2 cells after CCS treatment were measured by Real-time PCR. The above RNA products were examined by Agarose Gel Electrophoresis (C). The expression levels of M1 phenotype markers IL-1β, TNF-α, iNOS

and M2 phenotype markers IL-10, TGF-β, Arg1 in LPS+IFNγ-induced BV2 cells after CCS treatment were measured by Western Blotting (D). The decreased CD86 (E) and increased CD206 (F) were detected in LPS+IFNγ-induced BV2 cells after different concentrations of CCS by Flow Cytometry. The co-localizations and expressions of microglial marker Iba-1 with CD86 (G) or CD206 (H) in LPS+IFNγ-induced BV2 cells after CCS treatment were measured by Immunofluorescence. The NGF was co-localized with microglial marker Iba-1 by Immunofluorescence (I). The transcription of NGF in LPS+IFNγ-induced BV2 cells after CCS treatment was measured by Real-time PCR (J), and the RNA products were examined by Agarose Gel Electrophoresis (K). The expression and secretion of NGF in LPS+IFNγ-induced BV2 cells after CCS treatment were measured by Western Blotting (L) and ELISA (M). *P<0.05, **P<0.01, ***P<0.001, compared with Control group; #P<0.05, ##P<0.01, ###P<0.001, compared with LPS+IFNγ group.

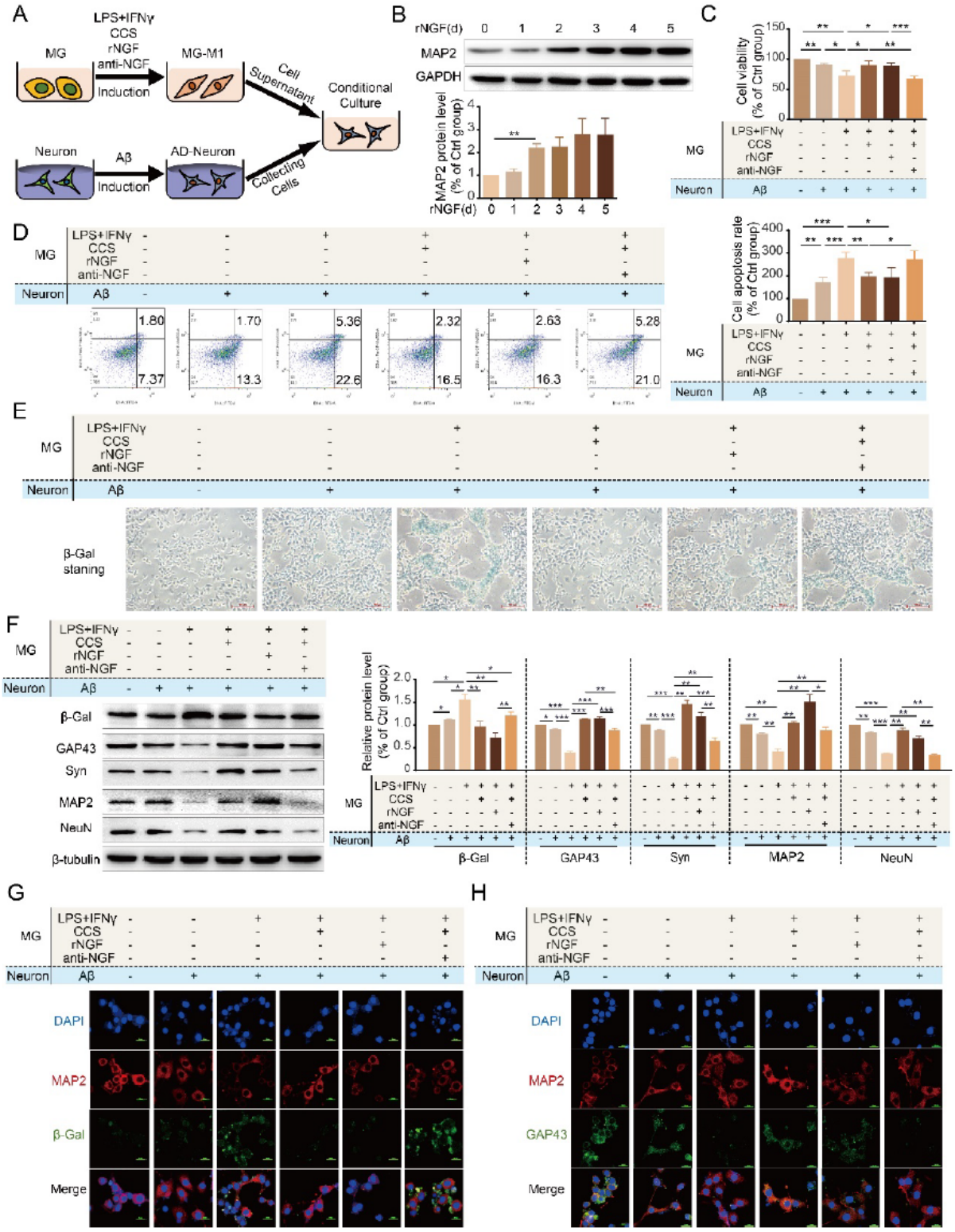

Figure 4

MG-derived NGF was the pivotal factor in the neuronal microenvironment to improve the Aβ1-42-induced neuronal senescence and plasticity after CCS-induced MG-M2 polarization. The pattern diagram of cultured AD neurons in the supernatant of the LPS+IFNγ group treated with different treatments (A). rNGF recombinant protein induced the differentiation of PC-12 cells into neuron cells (B). The cell viability (C) and apoptosis (D) of AD neurons with CCS treated-conditional medium were investigated by CCK8 assay

and Flow Cytometry. The senescence of AD neurons with CCS treated-conditional medium was investigated by β-Gal Assay (E). The expressions of β-Gal、GAP43、Syn、MAP2、NeuN in the AD neurons with CCS treated-conditional medium were measured by Western Blotting (F). The co-localizations and expressions of neuron marker MAP2 with β-Gal (G) or GAP43 (H) in the AD neurons with CCS treated-conditional medium were examined by Immunofluorescence. *P<0.05, **P<0.01, ***P<0.001, compared with counter group.

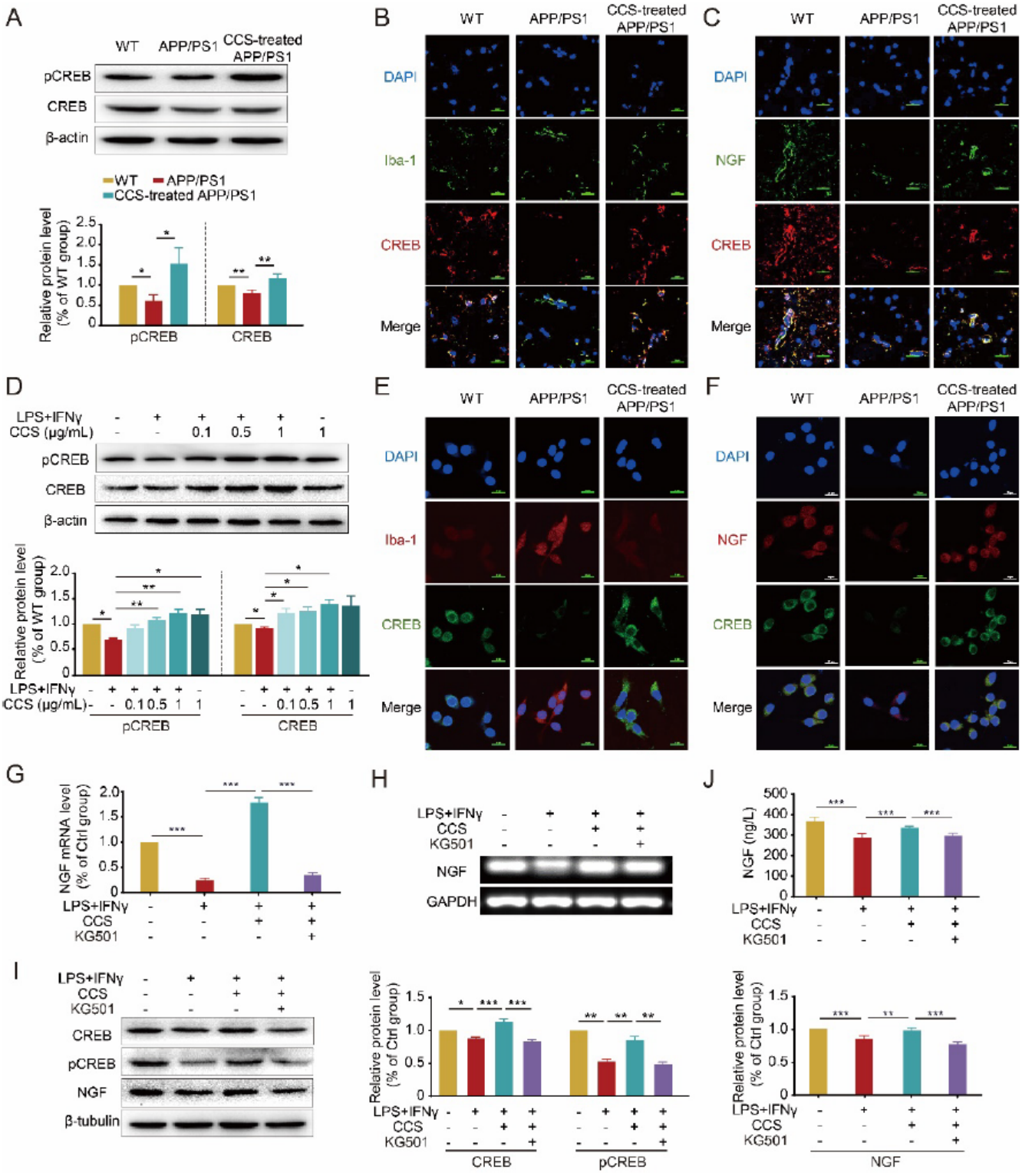

Figure 5

CCS treatment increased NGF levels after inducing microglial M2 polarization attributed to CREB activation. The expressions of CREB and phosphorylated CREB (pCREB) in the hippocampus of APP/PS1 mice treated with CCS were measured by Western Blotting (A). The co-localizations and expressions of CREB with microglial marker Iba-1 (B) or NGF (C) in the hippocampus of APP/PS1 mice treated with CCS were examined by Immunofluorescence. The expressions of CREB and pCREB in the LPS+IFNγ-induced BV2 cells after CCS treatment were measured by Western Blotting (D). The co-localizations and expressions of CREB with microglial marker Iba-1 (E) or NGF (F) in LPS+IFNγ-induced BV2 cells after CCS treatment were examined by Immunofluorescence. The transcription of NGF in BV2 cells treated with KG501, which is the specific inhibitor of CREB, was measured by Real-time PCR (G). The above RNA products were examined by Agarose Gel Electrophoresis (H). The expressions of CREB, pCREB, and NGF in BV2 cells treated with KG501 were measured by Western Blotting (I). The secretion of NGF in BV2 cells treated with KG501 was measured by ELISA (J). *P<0.05, **P<0.01, ***P<0.001, compared with counter group.

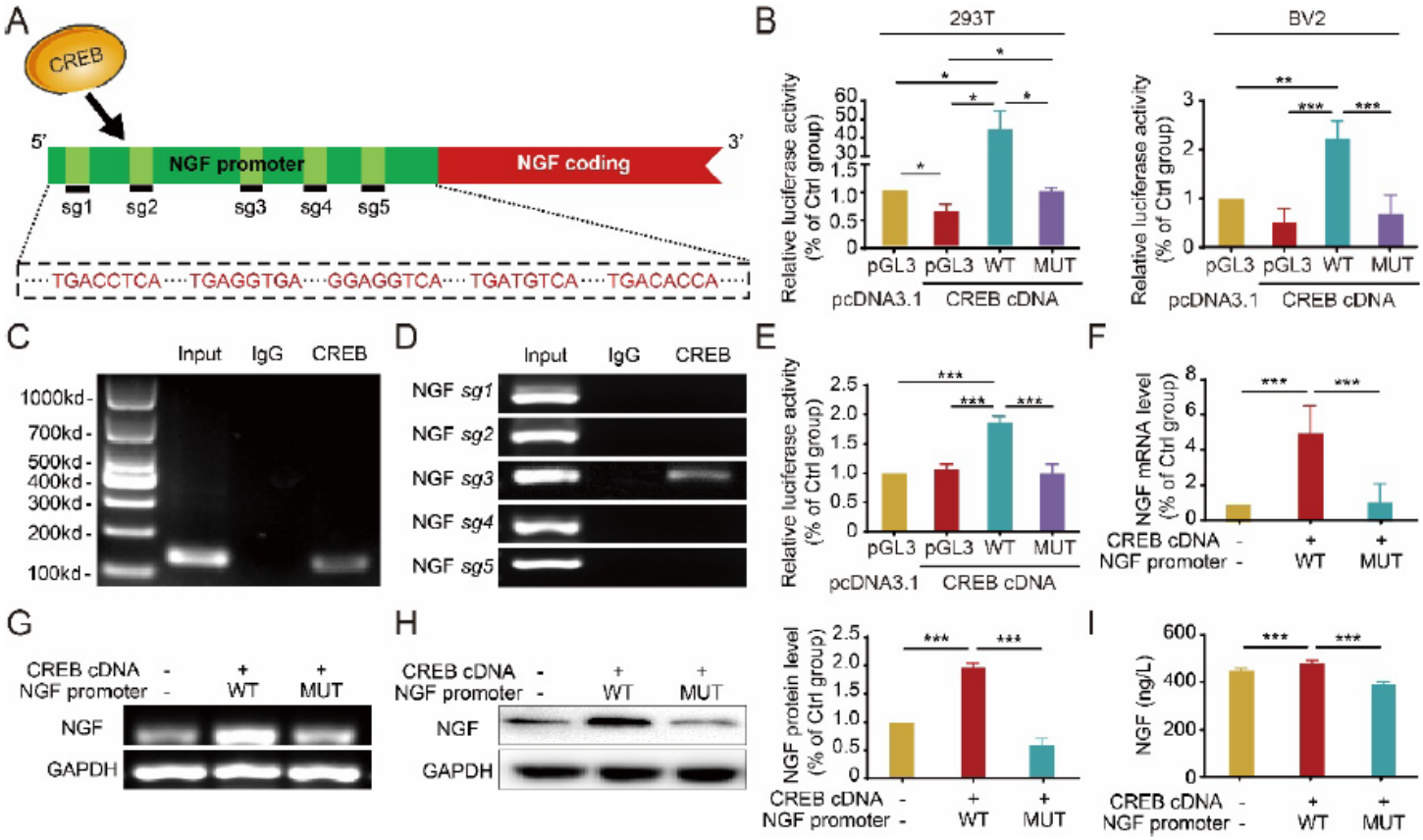

Figure 6

CREB bound with the key binding site sg3 (-1018~-1011) of NGF promoter to promote NGF transcription, expression, and secretion. Five key binding sites for transcription regulator factor CREB to bind with the NGF promoter region were predicted by JASPER Online Biological Prediction Website (A). The binding intensity of the CREB and NGF promoter region was examined in 293T and BV2 cells, respectively, by Luciferase Reporter Assay (B). The combination of CREB and NGF promoter region was investigated by ChIP Assay (C). The combination of CREB and different sites in the NGF promoter region were

investigated by ChIP Assay, including sg1 (-1381~-1374), sg2 (-1135~-1128), sg3 (-1018~-1011), sg4 (-425~-418), and sg5 (-218~-211) (D). The binding intensity of CREB and the third binding site (sg3) in the NGF promoter region was examined by Luciferase Reporter Assay (E). The transcription of NGF in the BV2 cells treated with double-transfection was examined by Real-time PCR (F). The above RNA products were examined by Agarose Gel Electrophoresis (G). The expression of NGF in the BV2 cells treated with double-transfection was measured by Western Blotting (H). The secretion of NGF in the BV2 cells treated with double-transfection was measured by ELISA (I). *P<0.05, **P<0.01, ***P<0.001, compared with counter group.

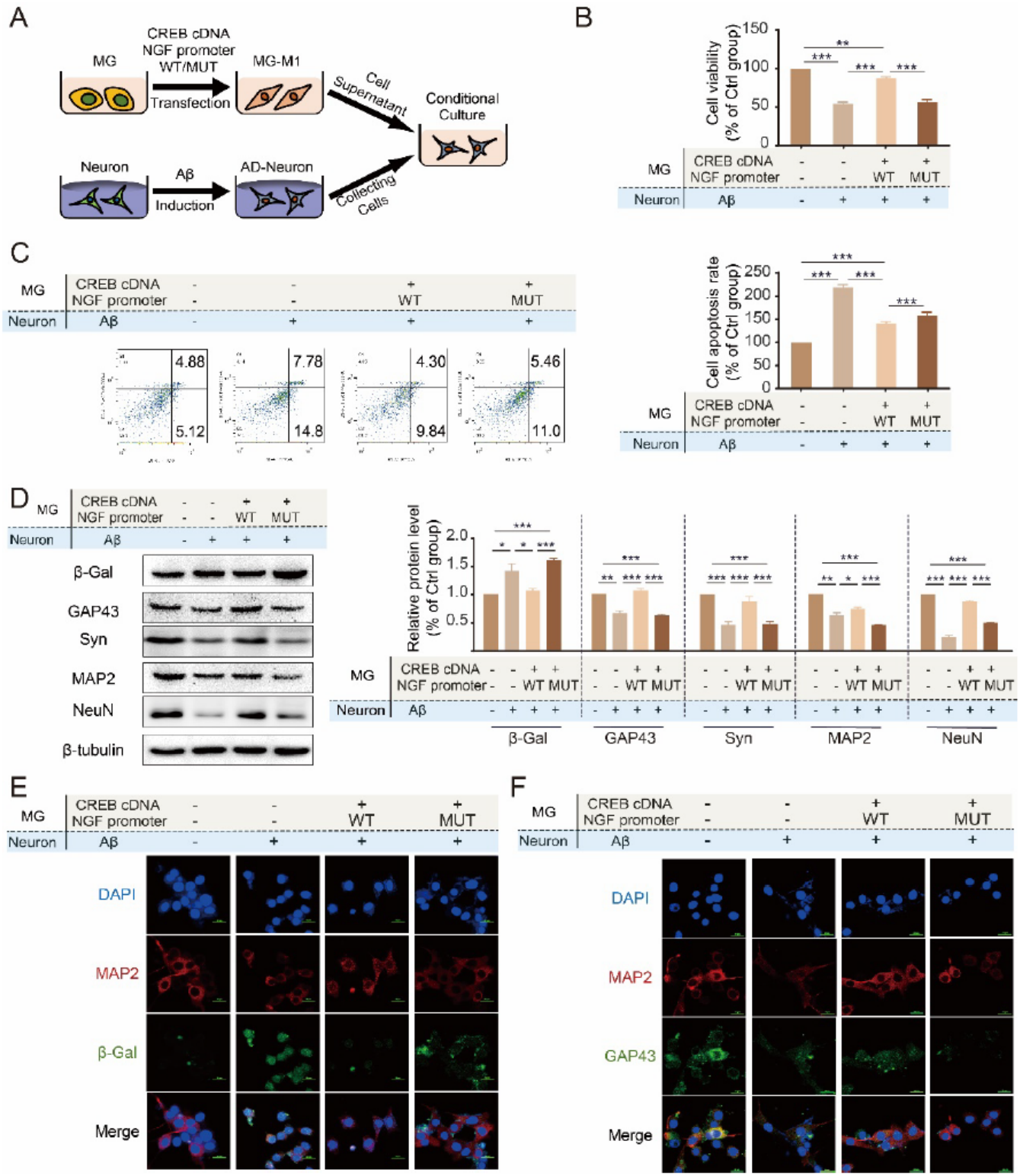

Figure 7

CREB bound with the key binding site sg3 (-1018~-1011) of NGF promoter to promote NGF transcription to mediate the neuronal plasticity. The pattern diagram of cultured AD neurons in the supernatant of BV2 cells treated with double-transfection (A). The cell viability (B) and apoptosis (C) of AD neurons with conditional culture were investigated by CCK8 Assay and Flow Cytometry. The expressions of β-Gal, GAP43, Syn, MAP2, and NeuN in the AD neurons with conditional culture were measured by Western

Blotting (D). The co-localizations and expressions of neuron marker MAP2 with β-Gal (E) or GAP43 (F) in the AD neurons with conditional culture were examined by Immunofluorescence. *P<0.05, **P<0.01, ***P<0.001, compared with counter group.

Supplementary Files

This is a list of supplementary files associated with this preprint. Click to download.

- Graphicfile.pdf